FirePhysChem xxx (xxxx) xxx

Contents lists available at ScienceDirect

FirePhysChem

journal homepage: http://www.keaipublishing.com/cn/journals/firephyschem/

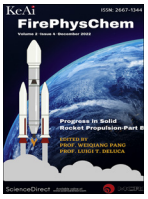

Array of carbon black-based microthrusters for CubeSat applications

A. Ingenito [a,*], S.K. Palateerdham [a], M. Panzanaro [b]

[a] School of Aerospace Engineering, La Sapienza, Rome, Italy
[b] TEC.R.A.S. tecnologia per ricerca ambiente e scuola, L'Aquila, Italy

ARTICLE INFO

Keywords:
Solid propellant
Microthruster
CubeSat
Propulsion
Combustion
Rocket

ABSTRACT

Access to space for small private companies requires to improve the ability to bring low-cost satellites into orbit. CubeSats offer a unique opportunity to meet these needs thanks to their reduced production times, the low manufacturing costs and ease of use. In order to be able to communicate with each other, exchange information and interact, it is necessary to place CubeSats in formation: in this context, miniature propulsion technologies, including chemical and electric propulsion, play a critical role in achieving mission requirements and maintaining satellites position. In this article, the feasibility of solid propellant micro rockets, fully integrated in an opposing array of printed thrust chambers is examined: each rocket can be fired together with the others or separately to modulate thrust. Theoretical and experimental results show that the microthruster, made of nylon and carbon fiber, have good mechanical and thermal resistance and simultaneously good performance is achieved. In particular, a microthruster with a diameter of 4 mm and a length of 6 mm, with 55 g of black powder propellant, achieves a thrust of about 3.5 N for about 7 ms.

1. Introduction

Over the past three decades, the space launch market has experienced a continuous increase in the average annual rate of launches. In 2013 only 247 CubeSats and 105 small non-CubeSat satellites were launched worldwide representing less than 2% of the entire mass launched so far, according to the Space Report of the 2022 edition. After 2013, the number of small satellites has increased significantly, by more than 30% per year, and it is the primary way of accessing space for private and academic institutions. In 2020, 94% of the 1284 spacecraft launched were small launchers, with a total payload of 600 kg. Out of these 600 kg, 28% of the payload was less than 200 kg and 9% was composed of nanosatellites. This miniaturization allowed the introduction of a new concept of space mission for earth observation, based on a constellation or formation of flying microsatellites. The challenge of forming flying microsatellites lies in the ability for a constellation of small satellites to interact with each other and work together to achieve the same performance as a single large satellite at lower expense, with faster production times and lower replacement costs. In this context, a key point of these microsatellite constellations is the possibility of providing them with micro-thrusters, to guarantee very small and very precise forces to obtain their stabilization, pointing and maintenance. Propulsion systems capable of delivering small and precise impulses, of the order of 1 μNs to 1 mNs, should be envisaged to overcome aerodynamic drag and keep the microsatellite in the right position of the flight formation. The goals of this paper are 1. To investigate the scaling of thermo-fluid-dynamic physical mechanisms interaction due to the thruster miniaturization; 2. To investigate the performance of a low-cost carbon black micro-rocket; 3. To propose a configuration of an array of multiple ignition thrusters for future applications to clusters of microsatellites in formation.

2. Scaling laws for microthrusters

The miniaturization of satellites requires a corresponding miniaturization of propulsion systems. Understanding how thruster performance scales with the engine size is critical. To date, few papers discuss in depth the scaling of physical laws for rocket applications [1–5].

When shrinking a chemical rocket, assuming the diameter of the same order of magnitude of the length, i.e., $D/L \sim$ O (1), the ratio between the surface area, proportional to $\sim L^2$, and the volume, proportional to $\sim L^3$, grows $\sim 1 / L$. Since the thrust T scales with the area, as shown in Eq. (1):

$$Thrust = \dot{m}U_e = \rho\pi\frac{D^2}{4}\sqrt{\frac{2\gamma\Re}{\gamma-1}\frac{T_g}{MW}\left(1-\left(\frac{p_e}{p_c}\right)^{\frac{\gamma-1}{\gamma}}\right)} \quad (1)$$

and the weight scales with the volume (see Eq. (2)):

$$W = \mathrm{rV} \quad (2)$$

it follows that the thrust/weight ratio, T/W, increases: this is a very interesting trend. However, on very small scales, combustion may not be able to be established and maintained and may be affected by the phenomenon of quenching. In fact, as the diameter decreases, the surface of

* Corresponding author.
E-mail address: antonella.ingenito@uniroma1.it (A. Ingenito).

https://doi.org/10.1016/j.fpc.2023.01.001
Received 2 September 2022; Received in revised form 24 January 2023; Accepted 28 January 2023
Available online xxx

Nomenclature

a, b	Ballistic coefficients
A_b	Microthruster burning area (m^2)
A_e	Nozzle exit area (m^2)
A_T	Nozzle throat area (m^2)
c^*	Characteristic Velocity (m/s)
Cf	Thrust coefficient
CC	Combustion chamber
D	Thruster characteristic diameter (m)
h	Heat transfer coefficient (W/(m^2K))
I_{sp}	Specific impulse (s)
k	Thermal conductivity (W/(m·K))
L	Thruster characteristic length (m)
$\dot{m}$	Mass flow rate (kg/s)
MW	Molecular weight (kgmole/kg)
M	Mach number
P_e	Nozzle exit pressure (Pa)
P_c	Combustion chamber pressure (Pa)
P_r	Prandtl number
r_b	Burning rate (cm/s)
R_e	Reynolds number
T_{thrust}	Thrust (N)
T_g	Thruster chamber temperature (K)
T_w	Thruster chamber wall temperature (K)
T_c	Combustion chamber temperature (K)
U	Average velocity in rocket chamber (m/s)
U_e	Nozzle exit velocity (m/s)
V	Volume (m^3)
W	Weight (kg)
W_{tot}	Total power (W)
W_{sp}	Power/unit volume (W/m^3)
W_{wall}	Power lost through the wall (W)

Greek letters

γ	Specific heat ratio
μ	Molecular viscosity (kg/(m·s))
ρ	Density (kg/m^3])
$\Re$	Gas constant (J/(K·mol))

Subscripts

b	Burn
c	Combustion chamber
e	Exit
sp	Specific
T	Throat
tot	Total

the grain and the internal volume of the combustion chamber are also reduced, but at different rates: therefore, the ratio between surface and volume increases with decreasing diameter. The heat produced per unit volume may be less than the heat required per unit area to vaporize the fuel. This can result in a flame that is unable to provide enough heat to vaporize the surrounding fuel, thus extinguishing the flame. In addition, the behavior of thermos-fluid dynamic physical mechanisms that contribute to the performance of the thruster, such as residence time, heat release, heat transfer, viscous effects, must also be considered.

Scaling rockets, the residence time decreases, and this could affect the efficiency of combustion; at the same time the surface/volume ratio increases, increasing thermal losses and the Reynolds number decreases increasing the friction losses. In fact, although usually the viscous effects do not have such a substantial influence on inertial forces and the flow is assumed to be ideal in first approximation, decreasing the size implies a decrease in the Reynolds number. Also, as the pressure decreases, the Reynolds number decreases further. For example, at the outlet of the nozzle, assuming $p = 10$ bar, the corresponding Reynolds number is approximately (Eq. (3)):

$$\mathrm{Re} = \frac{\rho \mu D}{\mu} = \frac{5 \times 10^{-1} \times 1000 \times 100 \times 10^{-6}}{10^{-4}} = 500 \tag{3}$$

As a result, the contribution of viscous forces becomes increasingly important, and the flow may no longer be considered ideal, isentropic expansion hypotheses may no longer be valid and need to be revised. A loss factor should be implemented in order to reduce real performance compared to the prediction of the ideal case. In fact, experimental tests in small resistojets [6] with Area Ratio = 100 and Re = 200–300 have shown an I_{sp} of the order of 70 s instead of the theoretical 130 s, demonstrating that the traditional sizing is insufficient to correctly predict the thruster performance and an experimental campaign or very precise simulation is required to understand the "right" physics and avoid costly mistakes in micro-thruster design.

In addition, the reduction in the size of the thruster leads to ever higher thermal loads on the walls of the chamber, making the walls hotter. In fact, the total power generated by the rocket scales with the volume, as shown in Eq. (4):

$$W_{tot} = W_{sp} \frac{\pi D^3}{4} \tag{4}$$

whereas the power lost through the walls scales with the surface, as shown in Eq. (5):

$$\begin{aligned} W_{wall} &= h \pi D L (T_g - T_w) \\ &= k Re^{1/2} Pr^{1/3} \pi D (T_g - T_w) \sim k \left(\frac{\rho u D}{\mu} \right)^{1/2} Pr^{1/3} \pi D (T_g - T_w) \end{aligned} \tag{5}$$

In Eq. (5), only the contribution due to convection is accounted for. A better analysis should include radiative heat transfer in series with the convection: however, at relatively larger sizes, the "bottleneck" is the radiative heat, while at smaller sizes, the heat transfer control will shift to convection.

The heat flux through the walls can be calculated by Eq. (6):

$$\frac{W_{wall}}{D^2} = \left(\frac{\rho u}{\mu} \right)^{1/2} Pr^{1/3} \pi D^{-\frac{1}{2}} (T_g - T_w) \tag{6}$$

Eq. (6) shows that heat flux increases with $1/\ D^{\frac{1}{2}}$. Therefore, the reduction in the size of the thruster leads to high thermal loads on the walls of the chamber. In this context, the walls become critical regions of the engine. This effect is compensated by the very short combustion times usually of the order of a few ms. In fact, increases in operating time can induce prohibitive thermal load and therefore deformation of the structure.

In addition, previous considerations have been done assuming the still valid continuum hypothesis, i.e. the Knudsen number, $Kn = \Lambda / L$ (where Λ is the mean free path of the gas molecule and L is a characteristic length scale) is still much less than 1. In Ref. [7], the Knudsen number is simply calculated by Eq. (7):

$$Kn = \sqrt{\frac{\gamma \pi}{2}} \frac{M}{Re} \tag{7}$$

where, again, M is the Mach number and Re is the Reynolds number of the flow. Kn of order of 0.01 – 0.1 is a representative range of values in which rarefaction effects begin to appear: therefore, this hypothesis must be verified.

3. Solid rocket propellants selection

When selecting the solid propellant formulations suitable for micro-rockets, several aspects need to be taken into account [8–12]:

1. Manufacturing and replicability;
2. Cost;

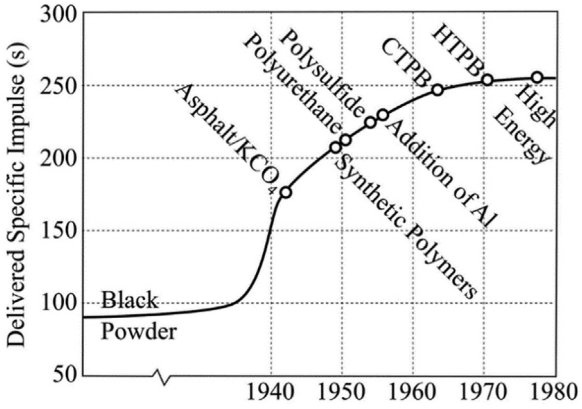

Fig. 1. I_{sp} of different propellants [8,13].

3. Regression rate;
4. Specific impulse;
5. Scaling effect.

Although the black powder is relatively inexpensive and readily available, Fig. 1 [8,13] shows that it has a relatively low specific impulse when compared with all other castable propellants; see also [14].

For instance, the ideal specific impulse analytic expression is:

$$I_{sp} = \sqrt{\frac{2\gamma\Re}{\gamma - 1}\frac{T_g}{MW}\left(1 - \left(\frac{p_e}{p_c}\right)^{\frac{\gamma-1}{\gamma}}\right)} \tag{8}$$

This equation shows that I_{sp} depends on the adiabatic flame temperature and the molecular weight of the combustion products. Solid composite propellants, or even castable composites, based on ammonium perchlorate, a fuel and a binder, exhibit superior performance capabilities and superior physical properties; however, these improvements are achieved at the expense of simplicity in fuel grain processing. In fact, the production process of castable propellants is expensive and time-consuming, while for the black powder, which is granular and pressable, the production process can be easily automated by multiple hydraulic power machines. Furthermore, as the size decreases, casting the more performing propellants becomes more difficult due to their high viscosity while in liquid form. In this study, therefore for simplicity of implementation, costs and time, black powder was chosen as a propellant to study the feasibility of these micro-rockets and their performance.

4. Black powder theoretical performance

Black powder is a mix of three different components. It consists of potassium nitrate (75% by weight), carbon (15% by weight) and sulfur (10% by weight). Each of these components plays an important role in combustion. In fact, potassium nitrate decomposes at a high temperature to provide oxygen for the reaction, sulfur undergoes exothermic reactions at relatively low temperatures, providing more energy and lowering the ignition temperature of the carbon. The performance of the carbon black powder has been calculated by means of the NASA CEA code 600 [9]. Fig. 2 shows that the adiabatic flame temperature ranges from $T = 1670$ K at $P_c = 1$ bar to $T = 1890$ K at $P_c = 20$ bar. When the pressure increases from 1 bar to 5 bar, the temperature increases by 8% and from that onwards the increase is less steep. In fact, increasing the pressure from 5 bar to 20 bar, the temperature increases by 3%, that is, from 1820 K to 1890 K.

As for the I_{sp}, Fig. 2 shows that it increases from 500 m/s at $P_c = 1$ bar to 1000 m/s at $P_c = 5$ bar, then it keeps constant at 1000 m/s from 5 bar to 20 bar. This is due to the increase in the molecular weight (see Fig. 3) of the products which compensates the increase in temperature in the pressure range between 5 bar and 20 bar as shown in Fig. 3.

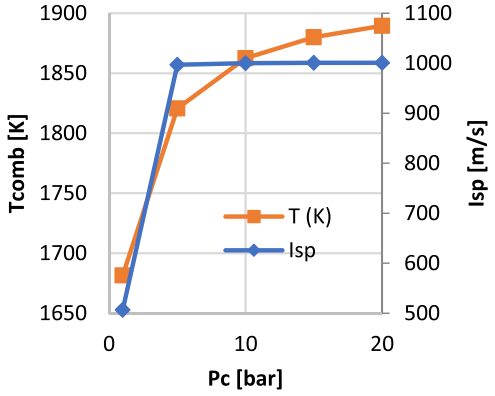

Fig. 2. Combustion temperature T_c and I_{sp} vs P_c.

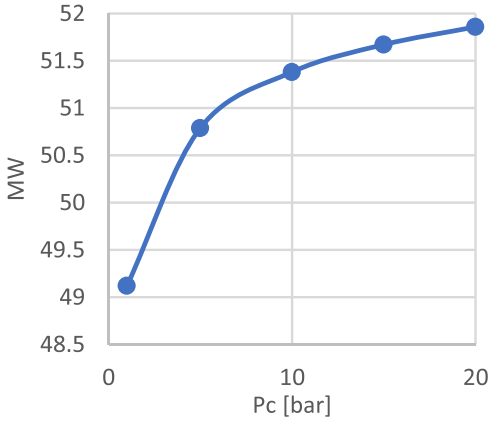

Fig. 3. MW vs P_c.

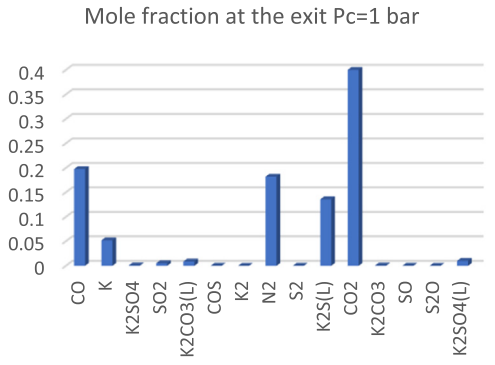

Fig. 4. Mole fraction in CC at $P_c = 1$ bar.

The combustion products in the combustion chamber (CC) consist mainly of CO, N_2, K_2S, CO_2, K, K_2CO_3 and K_2SO_4 (see Figs. 4–7). From the composition of the combustion products, obtained by assuming stoichiometric conditions, a simplified equation for the reaction of black powder can be identified:

$$10KNO_3 + 10C + 3S \rightarrow 2K_2CO_3 + 2K_2SO_4 + 6CO_2 + 5N_2 + 2CO + K_2S + SO_2$$

At $P = 1$ bar, the flow temperature in the diverging part of the nozzle decreases by more than 50 K below the condensation temperature of some products. This causes erosion problems in the nozzle throat, and also very low performance: therefore, atmospheric pressure in the combustion chamber must be discarded.

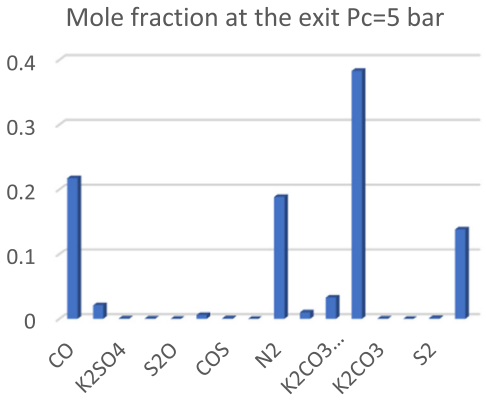

Fig. 5. Mole fraction in CC at $P_c = 5$ bar.

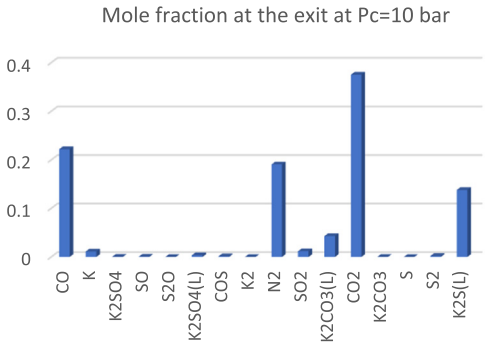

Fig. 6. Mole fraction in CC at $P_c = 10$ bar.

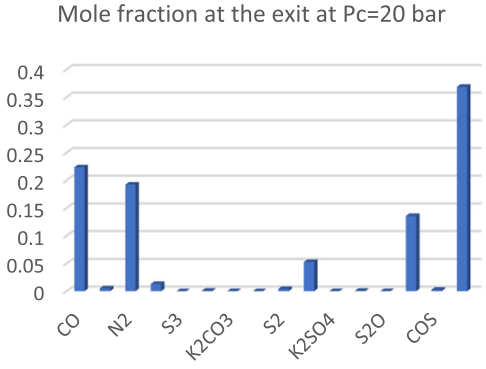

Fig. 7. Mole fraction in CC at $P_c = 20$ bar.

The ideal thrust coefficient, *Cf*, given by Eq. (9):

$$Cf = \frac{Thrust}{P_c A_t} = \gamma\left(\frac{2}{\gamma+1}\right)^{\frac{\gamma+1}{2(\gamma-1)}}\left\{\frac{2\gamma}{\gamma-1}\left[1-\left(\frac{P_e}{P_c}\right)^{\frac{\gamma-1}{\gamma}}\right]\right\}^{1/2} + \left(\frac{P_e}{P_c}-\frac{P_a}{P_c}\right)\frac{A_e}{A_t} \quad (9)$$

has been theoretically calculated by the CEA code (see Fig. 8). Once *Cf* is known, the thrust may be theoretically predicted by Eq. (10):

$$Thrust = Cf \cdot P_c \cdot A_t \quad (10)$$

Fig. 9 shows that, assuming a pressure expansion ratio of 10 for all cases, as the chamber pressure increases, the thrust increases going from 50 mN at $P_c = 1$ bar, to 2 N at $P_c = 20$ bar.

By increasing the pressure expansion ratio from 10 to 30, Fig. 10 shows that the thrust coefficient *Cf* and the specific impulse increase by approximately 18%. Under steady operation, the equilibrium pressure in the combustion chamber may be calculated by Eq. (11) [15,16]:

$$P_c = \left(\frac{A_b}{A_t} a.\rho.c^*\right)^{\frac{1}{1-n}} \quad (11)$$

where, P_c is in Pascal, A_b and A_t are respectively the burning and the throat area in m^2, a and n are the ballistic coefficients, ρ is the density in kg/m^3 and c^* is the characteristic velocity in m/s. From this equation, assuming a cigarette grain geometry, with a burning area diameter of 4 mm and a throat diameter of 1 mm, the pressure in the combustion chamber is about 12 bar. Fig. 11 shows that at this pressure, the regression rate, calculated by implementing the parameter reported in Table 1, is approximately 26.9 cm/s for black powder grain and 9.2 cm /s for castable fuels.

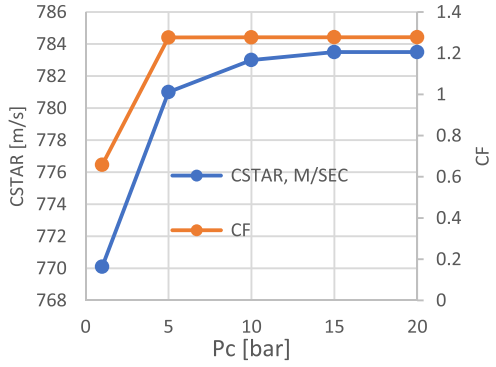

Fig. 8. *Cf* and c^* vs.

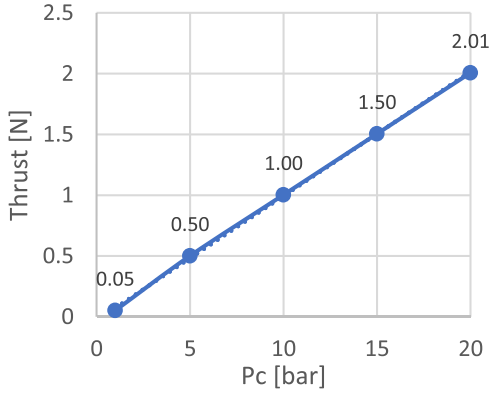

Fig. 9. Thrust vs P_c.

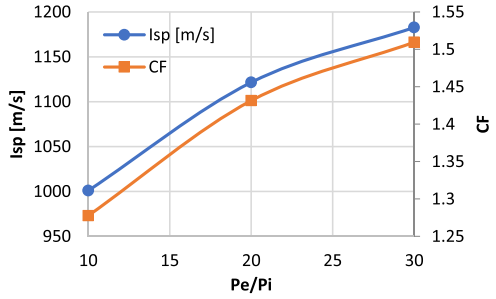

Fig. 10. *Cf* and I_{sp} vs P_e /P_i at $P_c = 20$ bar.

5. Black powder experimental results

In this section, experimental tests and results are reported. The micro-rocket consists of an ignition system (in green), the combustion

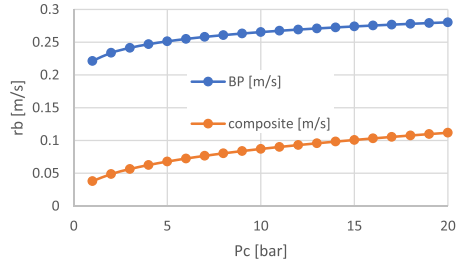

Fig. 11. *BP* and composite grain regression rate vs P_c.

Table 1
regression rate of solid propellants [15].

	Burn rate	Burn rate exponent	Burn rate coefficient
Black powder	$r_b = 18.16\ (P_c/6895)^{0.08}$	0.05–0.11	0.50–0.70
Castable fuels	$r_b = 1.46\ (P_c/6895)^{0.36}$	0.32–0.70	0.02–0.06

In Table 1, r_b is in cm/s and P_c in MPa.

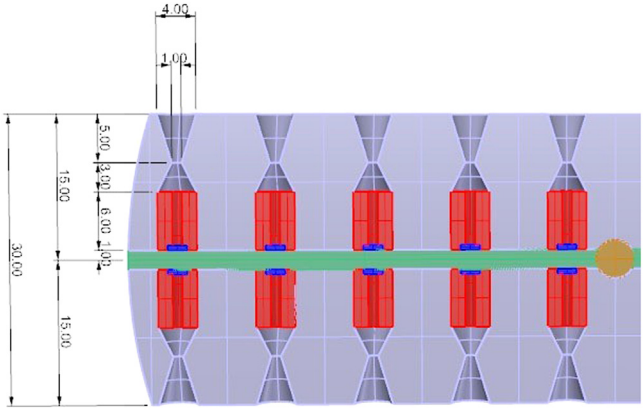

Fig. 12. 2D view of the micro-rockets array.

Fig. 13. Photos of a single microrocket.

chamber (in red) and the micronozzle through which the exhaust gasses escape (in purple). A schematic of the microrockets array is reported in Fig. 12.

1. The geometry of a single micro rocket consists of:
2. Inner diameter 4 mm
3. Nozzle throat diameter 1 mm
4. Chamber length 6 mm

The micro-rocket is designed in CAD, as shown in Fig. 12, then made in house with a high-modulus carbon fiber nylon, by means of a 3D printer (see Fig. 13). This material has the advantage of superior thermal, mechanical and chemical resistance properties, while maintaining ease of printing and very low weight. The total weight of the engine is 453 mg.

The black powder (*BP*) consists of grains of about 1 mm. It is filled by pressing it in the combustor. Experimental tests have been carried out for three different amounts: 25 mg, 55 mg and 80 mg; a small quantity of about 5 mg with potassium chlorate instead of potassium nitrate has been chosen for the ignition system.

Fig. 14 shows the experimental setup: the thrust is measured using a load cell of a digital scale with a capacity of 200 g, and a sensitivity of 0.01 g. The signal has been taken directly from the load cell, amplified and recorded with a Rigol DS1202 oscilloscope.

An experimental test campaign was conducted for 3 different masses of propellant grain: 25 mg, 55 mg 80 mg. For each test, 5 tests were conducted. The measured error of thrust follows the same trend for all three cases, i.e., the error is about 15% in the first 0.6 ms, then reduces to 3% and then re-increases to 8% near the thrust peak. The error then reduces again to 3% and then increases again to 8% in the last 0.5 ms. All the figures show a average value of the results in function of the time. The history of the thrust is shown in Fig. 15. After 20 ms from the ignition, the thrust increases reaching 1 N, 3.5 N and 4 N burning respectively 25 mg, 55 mg and 80 mg of black powder. Fig. 15 shows that the burning time is approximately the same for all cases, i.e. about 7.4 ms, while the thrust increases with the mass of the propellant. For the same geometry of the engine, and the same throat area of the nozzle, the mass flow rate of the propellant varies from 3.3 g/s at 7.3 g/s and 10 g/s: this implies an increase in the pressure in the combustion chamber. This increase in pressure, with the same grain geometries, can be explained by assuming a rapid heat transfer to the grain that favours its chemical kinetics, therefore the grain regression rate, therefore the increase in the mass flow rate of the exhaust gasses and consequently the increase of pressure in the combustion chamber.

Assuming a thrust coefficient of 1.27 (see Section 4), the experimental pressure in the combustion chamber can be calculated from Eq. (7), that is $P_c = \frac{T}{Cf \cdot A_t}$. Fig. 16 shows that the pressure has a maximum of about 12 bar after 4 ms from the ignition of the grain which occurs 20 ms after the ignition of the small quantity of pyrotechnic mass (see Fig. 15). By increasing the mass from 25 mg to 55 mg and then to 80 mg, the pressure increases from 12 bar to 35 bar and 40 bar. The thrust produced by the combustion of 25 mg of propellant, corresponding to a peak of 12 bars, is 1 N, which confirms the theoretical data provided in Fig. 9 (about 1.2 N).

The regression rate predicted in Fig. 11, assuming as reference pressure the peak pressure of 12 bar (see Fig. 16), is approximately 269 mm/s. Since the grain lengths are, respectively, 1 mm when the combustor is loaded with 25 mg, 2.5 mm for 55 mg and 3.7 mm for 80 mg of propellant, the burning time theoretically predicted is approximately 4.5 ms. Experimental data show a burning time of about 7.8 ms, with a discrepancy of about 40%: this disagreement may be explained considering that the pressure is not constant during the combustion and 12 bar is the peak value. For 55 mg of propellant, the theoretical burning time is 8 ms: in this case, the error is about 2.5%. For 80 mg, the theoretical burning time is approximately 11 ms, with an error of approximately 40%. Theoretical prediction overestimates the burning time when increasing the grain length and underestimates it when decreasing the grain length. This may be explained with the effect of the heat transfer to the wall when shrinking the rocket. In fact, for the same geometry of the rocket (see Fig. 12), having assumed for the grain a cigarette shape, as the length of the grain increases, the initial volume of the combustion chamber reduces, increasing the S/V ratio and therefore the heat losses to the walls, this consequently increases the regression rate compared to the theoretical case. The experimental results show that since the times are very short, the structure does not deform due to heat transfer to the wall, and the throat keeps a size of 1 mm.

For the measured thrust (see Fig. 15), the experimental U_e, shown in Fig. 17, is about 1200 m/s, corresponding to what is predicted in Figs. 1 and 10.

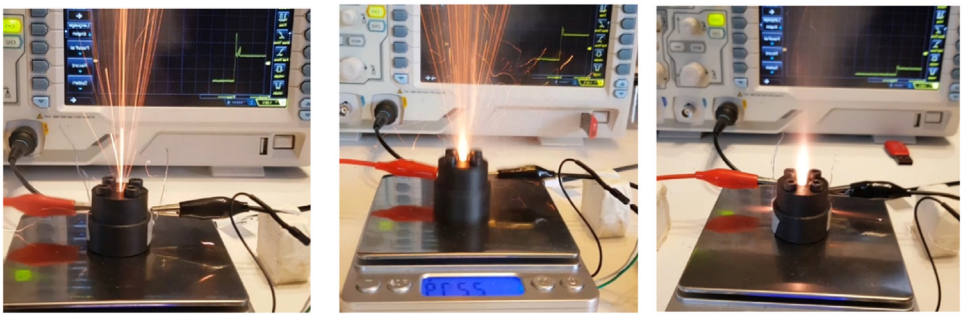

Fig. 14. *BP* experimental test for 25 mg, 55 mg, 80 mg of propellants.

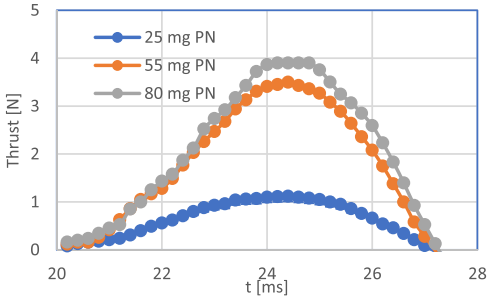

Fig. 15. Thrust vs time (ms).

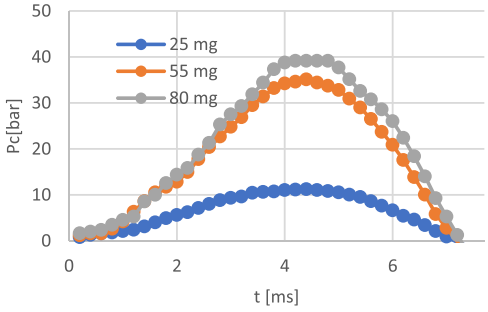

Fig. 16. P_c (bar) vs time (ms).

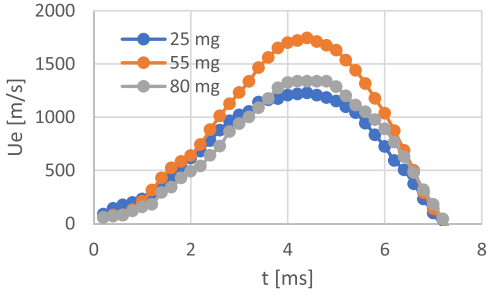

Fig. 17. U_e (m/s) vs time (ms).

6. Design and layout of the array of black powder microrockets

The current challenge for the future cluster of satellites in formation is to develop a system capable of operating multiple ignitions [17,18]. In the previous section, the feasibility of carbon black based microrocket has been demonstrated. In this section, possible configurations for CubeSat applications are suggested. The idea is to propose an array of opposing microrockets powered by carbon black propellant that can be combined in a 3U CubeSat of 10 cm × 10 cm × 30 cm (see Fig. 18).

The cluster configuration of opposing microrockets is shown in Fig. 19. Each plate contains 144 thrusters, for a total of 288 thrusters.

Fig. 18. Schematic view of the microrockets assembly.

These engines can be switched on simultaneously or separately through the electrical resistance placed in the central plate (in green) between the two opposing platforms. The ignition will depend on the desired module and direction of the thrust. The thruster's plate is divided into 4 plates of 36 motors each. Through a mechanical system, once all the motors of a single plate are turned on, it is possible to replace them with the opposite one.

The advantage of this configuration is that it is possible to modulate the thrust and direction of thrust through the ignition of one or more microrockets, at different positions that depend on the mission requirements. The minimum impulse bit is approximately 5 mNs for a grain of 25 mg, 13 mNs for 55 mg and 15 mNs for 80 mg. The total impulse of the whole array is 0.720 Ns, 1.87 Ns, 2.16 Ns for each side, respectively.

A thruster with 25 mg of *BP* produced a 1 N thrust for approximately 7.4 ms, while 55 mg and 80 mg of powder produced a thrust of 3.5 N and 4 N, respectively. The combustion time is approximately the same for all cases, i.e., about 7.4 ms, while the thrust increases with the mass of the propellant burned.

Assuming the combustion geometry and performance data reported in the previous sections:

Diameter = 0.004 m,
Length = 0.006 m,
Pressure in the CC =12 bar
Specific impulse = 120 s,

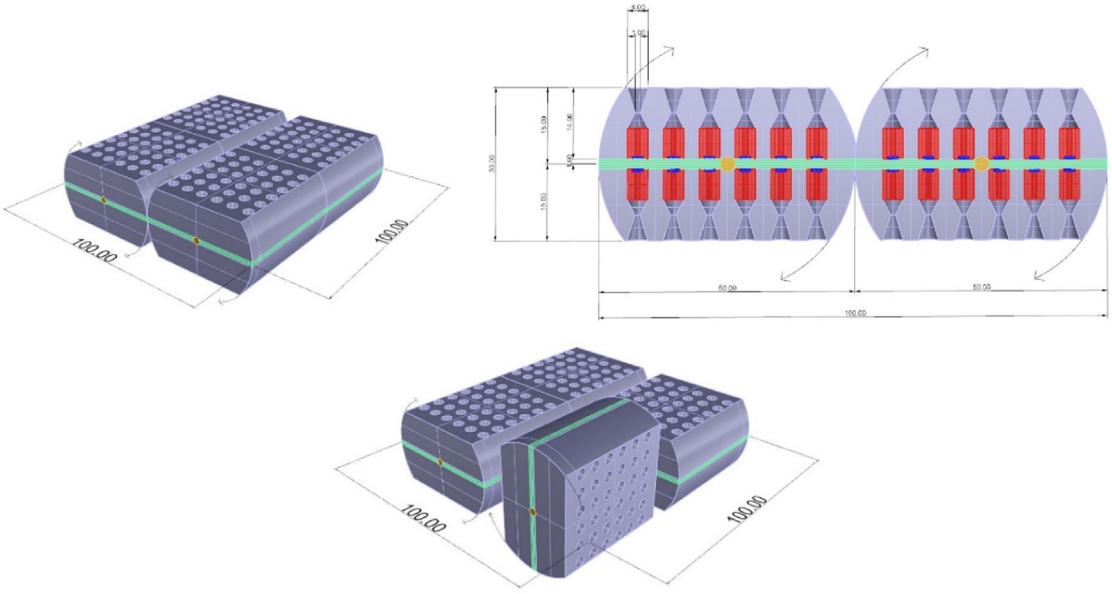

Fig. 19. Configuration of the microthrusters cluster.

Exit velocity = 1177.2 m/s,
Thrust = 3.5 N,
Mass flow rate = 0.08 g/s,

it can be concluded that with an array of 70 micro-rockets fired together, a DeltaV of 2.5 m/ s can be obtained in one shot, for 1 CubeSat of 3 kg.

These DeltaVs are sufficient to ensure good performance for the attitude control of small satellites within the constellation of microsatellites.

7. Conclusion

In this study, low-cost and highly efficient black powder-based micro-thrusters were theoretically and experimentally investigated for small satellite applications. Fused deposit model-based 3D printing technique is used to fabricate a micro-rocket. The theoretical performance and combustion products of Black Powder have been identified using the NASA CEA code. Although *BP* performance is lower than traditional fuels, its simplicity makes this propellant an attractive alternative to traditional castable propellants. These types of microrocket thrusters provide simplicity to the production process, operation, and market accessibility while lowering manufacturing costs. Additionally, they are renowned for their portability due to their ease of use, low waste production, and reduced power consumption, which enable them to maintain trajectory and maximize payload capacity. Experiments were conducted for three different cases of thrusters with different *BP* masses. A thruster with 25 mg of *BP* produced a 1 N thrust for approximately 7.4 ms, while 55 mg and 80 mg of powder produced a thrust of 3.5 N and 4 N, respectively. The combustion time is approximately the same for all cases, i.e., about 7.4 ms, while the thrust increases with the mass of the propellant burned. The data collected show that the use of propellants with fast burning times reduces the thrust losses due to the energy transfer to the combustion chamber walls and allows to obtain optimized models to size micro rockets according to the required performances. Theoretical predictions by CEA overestimates the experimental burning time when increasing the grain length and underestimates it when decreasing the grain length. This can be explained by the effect of heat transfer as the wall rises when shrinking the rocket. The experimental results confirmed that the traditional sizing is not sufficient to design correctly the engine and the development of a new theoretical model including these effects will be the subject of a future work by these authors. In addition, future work will include experimental work to evaluate the feasibility of such a microrockets array, investigating the ability to modulate thrust in modulus and direction as a function of a controlled ignition system.

Declaration of Competing Interest

The authors declare that they have no known competing financial interests or personal relationships that could have appeared to influence the work reported in this paper.

Reference

[1] P.N. Kadiresh, Prem C. Navaash, Ubaid Khan, Yoga Sundaram, Solid propellant–fuelled mirorocket for space application, Int. J. Ambient Energy 42 (11) (2021) 1223–1227 DOI: 10.080/01430750.2019.1587724.
[2] S. Schneider, G. Boyarko, C.J. Sun, Catalyzed ignition of bipropellants in microtubes, in: Proceedings of the 41st ASM, Reno, Nevada, 2003 6-9 January 2003.
[3] Alexeenko, A.A., Levin, D.A., Fedosov, D.A., Gimelshein, S.F., and Collins, R.J., (2003), “Coupled thermal and fluid analyses of michrothruster flows”, AIAA Paper 2003-0673, presented at the Proceedings of the 39th AIAA Joint Propulsion Conference, Huntsville, Al, 20-23 july 2003.
[4] Reed, B., (2003), “Decomposing solid micropropulsion nozzle performance issue”, AIAA Paper 2003-0672, presented at the Proceeding of the 41st Aerospazce Science Meeting, Reno, Nevada, 6-9 January 2003.
[5] Ketsdever, A.D., (2003), “Microfluidics research in MEMS propulsion systems”, AIAA Paper 2003-078, presented at the Proceeding of the 41st Aerospazce Science Meeting, Reno, Nevada, 6-9 January 2003.
[6] Schmitz, B. , Williams, D., SMITH W. and Maybee, D. (1976), "Development of design and scaling criteria for monopropellant hydrazine reactors employing shell 405 spontaneous catalyst", 2nd Propulsion Joint Specialist Conference, Colorado, Springs,13 - 17 June 1966, https://doi.org/10.2514/6.1966-594.
[7] W.F. Louisos, Alina A Alexeenko, Darren L. Hitt, A. Zilic, Design considerations for supersonic micronozzles, Int. J. Manuf. Res. TY 3 (2008), doi:10.1504/IJMR.2008.016453.
[8] M. Denny, A. McFadzean, Rocket propulsion and guidance, Rocket Science, Springer, Cham, 2019, doi:10.1007/978-3-030-28080-2_5.
[9] S. Gordon, B.J. Mcbride, in: Computer program for calculation of complex chemical equilibrium compositions and applications, NASA Reference Publication, 1996, p. 1311.
[10] I.K.U.T.A. Satoshi, H. Daichi, Y.A.N.O. Yasuyuki, K. Akira, Performance of a throttleable solid propellant microthruster using laser heating, Trans. Jpn. Soc. Aeronaut. Space Sci. Aerosp. Technol. Jpn. 19 (4) (2021) 598–603, doi:10.2322/tastj.19.598.
[11] A. Kakami (Ed.), Solid propellant microthruster. In book: Space Micropropulsion for Nanosatellites: Progress, Challenges and Future, edited by Kean How Cheah, 2022, doi:10.1016/B978-0-12-819037-1.00009-8.
[12] R.S. Fry. Solid propellant test motor scaling, 3 SEPTEMBER 2001, CPIA Report, No CPTR 73, https://apps.dtic.mil/sti/pdfs/ADA395610.pdf (dtic.mil).
[13] Umholtz P.D. (1999) The history of solid rocket propulsion and Aerojet, AIAA Paper 99–2927, 35th Joint Propulsion Conference and Exhibit, 20 - 24 June 1999, Los Angeles, CA, U.S.A. doi:10.2514/6.1999-2927.
[14] W.Q. Pang and L.T. DeLuca, editorial FPC, Vol. 2, Issue 1, March 2022, pp. 1–3

[15] S. Romero-Diez, L. Hantsche, J.M. Pearl, D.L. Hitt, M.R. McDevitt, P.C. Lee, A single-use microthruster concept for small satellite attitude control in formation-flying applications, Aerospace 5 (4) (2018) 119.
[16] A. Chaalane C. Rossi D. Estève, The formulation and testing of new solid propellant mixture (DB + x% BP) for a new MEMS-based microthruster, Sensors and Actuators A: Physical, Volume 138, Issue 1, 2007, Pages 161-166, ISSN 0924-4247, doi:10.1016/j.sna.2007.04.029.
[17] M.B. Kovac, R. Krishnan, J. Burton, M. Smith, R.J. Wood, Multi-stage micro rockets for robotic insects Mirko, Robot. Sci. Syst. (2012) 9 July, doi:10.15607/RSS.2012.VIII.024.
[18] E.A. Parra, K.J.S. Pister, C. Fernandez-Pello, Solid-propellant micro-thruster, The Sixth International Workshop On Micro and Nanotechnology for Power Generation and Energy Conversion Applications, Nov. 29 - Dec. 1, 2006, U.S.A.